# Sub-Planck-scale structures in the Pöschl-Teller potential and their sensitivity to perturbations

Utpal Roy,[1,*] Suranjana Ghosh,[1,†] Prasanta K. Panigrahi,[2,3,‡] and David Vitali[1,§]
[1]*Dipartimento di Fisica, Università di Camerino, I-62032 Camerino, Italy*
[2]*Indian Institute of Science Education and Research, Kolkata, India*
[3]*Physical Research Laboratory, Navarangpura, Ahmedabad, India*
(Received 2 April 2009; revised manuscript received 23 June 2009; published 24 November 2009)

We find the existence of sub-Planck scale structures in the Pöschl-Teller potential, which is an exactly solvable potential with both symmetric and asymmetric features. We analyze these structures in both cases by looking at the Wigner distribution of the state evolved from an initial coherent state up to various fractional revival times. We also investigate the sensitivity to perturbations of the Pöschl-Teller potential and we verify that, similar to the harmonic oscillator, the presence of sub-Planck structure in phase space is responsible for a high sensitivity to phase-space displacements.

DOI: 10.1103/PhysRevA.80.052115 PACS number(s): 03.65.−w, 42.50.Dv, 42.50.Md

## I. INTRODUCTION

The Wigner distribution $W(x,p)$ is a useful tool for visualizing quantum interference phenomena in phase space. Nonlocal superposition states show interference and the presence of phase-space regions where $W(x,p)$ is negative is an unambiguous signature of quantum behavior. The oscillatory structures resulting from quantum interference can have a dimension much smaller than the Planck's constant $\hbar$, and these sub-Planck scale structures were first found by Zurek in quantum chaotic systems [1]. Sub-Planck scale structures usually appear as alternate small "tiles" of maxima and minima. The phase-space area of these tiles are given by $\hbar^2$ divided by the effective phase-space area $A$ globally occupied by the state, which can be significantly larger than $\hbar$. These structures are very sensitive to environmental decoherence [1–6] and may have important application in Heisenberg-limited measurements and quantum parameter estimation [7,8]. A classical analog of sub-Planck scale structures, regarded as sub-Fourier sensitivity, has been studied in Ref. [9], and these structures have also been found in diatomic molecular systems [10], entangled cat state [11], optical fibers [12], and Kirkwood-Rihaczek distribution [13]. Recently, a connection between these structures and teleportation fidelity has been also established [14].

Sub-Planck structures have been extensively studied in the case of superpositions of harmonic oscillator coherent states and also for superpositions of generalized coherent states which occur in the time evolution of systems with nonlinear potentials at fractional revival times. It is therefore important to extend the study of this phenomenon to other nonlinear potentials in order to investigate which are the relevant parameters affecting this subtle quantum behavior, and if Heisenberg-limited sensitivity can be approached also in other nonlinear systems.

Here we focus our attention to the Pöschl-Teller (PT) potential, which has been applied to model various situations in recent years [15–19]. In fact, the PT potential has been used in the context of deep quantum wells, as well as for modeling optical systems with changing refractive index. The PT potential depends upon two parameters and by varying them one can switch from a symmetric to an asymmetric situation. Yildirim and Tomak studied in particular the nonlinear optical properties associated to the PT potential [18], and also the nonlinear changes in the refractive index resulting from its tunable asymmetry [19].

Another important feature of the PT potential is that it is exactly solvable and characterized by a quadratic spectrum: as a consequence its time evolution shows fractional revivals [20,21] and it may lead to the generation of linear superpositions of well distinct states in phase space. In this paper we confirm this expectation and find that an initial coherent state of the PT potential shows sub-Planck structures in phase-space at fractional revival times. We shall first study these structures when the PT potential is symmetric and then, by tuning the potential parameters, we switch to the asymmetric case in order to see the effects of the asymmetry on sub-Planck scale structures. In both cases we verify quantitatively that the dimension of the sub-Planck structures scales as $\hbar^2/A$, as expected, also for the PT potential.

We then study the sensitivity of sub-Planck scale structures to perturbations, by considering two different situations: (i) "internal" perturbations, i.e., a small change of the potential which is turned from symmetric into a slightly asymmetric one; (ii) "external" perturbations, as for example a weak force, yielding a small phase-space displacement of the state. Both cases will confirm that also in the PT potential, sub-Planck structures are responsible for a very high sensitivity to displacements.

The paper is organized as follows. In Sec. II, the symmetric and asymmetric properties of PT potential are reviewed and the revival dynamics of a coherent state (CS) wave packet are discussed. Existence of sub-Planck scale structures in phase space is demonstrated for both symmetric and asymmetric cases in Sec. III. In Sec. IV we discuss the sensitivity of sub-Planck scale structures due to a small asymmetry of the potential and then the one associated with a small phase-space displacement of the state. We end with some conclusions in Sec. V.

*utpal.roy@unicam.it
†suranjana.ghosh@unicam.it
‡prasanta@prl.res.in
§david.vitali@unicam.it

 

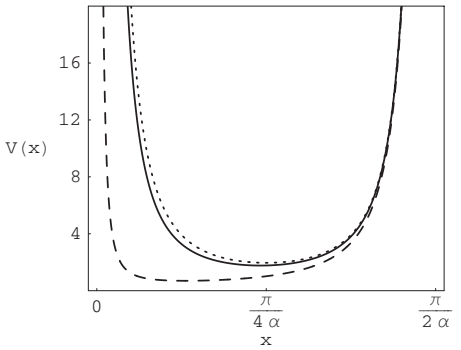


FIG. 1. The Pöschl-Teller potential V(x) (in unit of $10^4$ a.u.) for different parameter values. Dotted line represents the symmetric case ($\rho=\kappa=50$), solid line refers to the slightly asymmetric case ($\rho=50$, $\kappa=46$), while the strongly asymmetric case ($\rho=50$ $\kappa=6$) is shown by the dashed line. Here, the variable $x$ is in atomic units and we have chosen $\alpha=2$ a.u.

## II. PÖSCHL-TELLER POTENTIAL AND THE CS wave packet

The general PT potential [22] is given by

$$V(x)=\frac{\hbar^2\alpha^2}{2m}\left[\frac{\rho(\rho-1)}{\cos^2\alpha x}+\frac{\kappa(\kappa-1)}{\sin^2\alpha x}\right] \tag{1}$$

and it represents an array of potential wells in the whole line. The symmetric case can exhibit energy bands [23]. Since the wells are impenetrable, it suffices to consider only one of them for a full quantum mechanical description of the system. The potential is depicted in Fig. 1 for different values of $\rho$ and $\kappa$ $(\rho,\kappa>1)$ (units are chosen such that $\hbar=m=1$), and we have selected the well within the interval $[0,\pi/2\alpha]$. The dotted line corresponds to the symmetric well ($\rho=\kappa=50$), centered around $\pi/4\alpha$. This symmetric well smoothly takes the form of an infinite well in the limit of $\rho,\kappa\to 1$. The potential loses its symmetry with respect to the axis of the well if $\rho\neq\kappa$. Small and large asymmetries are shown, respectively, by the solid and dashed curves in Fig. 1. The minimum of the well is inclined toward the left side when $\rho>\kappa$.

The PT potential is one of the exactly solvable quantum mechanical potentials. The corresponding Schrödinger equation can be solved to obtain the energy eigenvalues and eigenfunctions [24]

$$E_n=\frac{\hbar^2\alpha^2}{2m}(2n+\rho+\kappa)^2,\quad n=0,1,2,\ldots$$

$$\psi_n(x)=N\cos^\rho(\alpha x)\sin^\kappa(\alpha x)P_n^{\rho-1/2,\kappa-1/2}[\cos(2\alpha x)], \tag{2}$$

where $P_n^{\rho-1/2,\kappa-1/2}[\cos(2\alpha x)]$ is the Jacobi polynomial and $N$ is the normalization constant,

$$N=\left[\frac{2\alpha\Gamma(n+1)(2n+\rho+\kappa)\Gamma(n+\kappa+\rho)}{\Gamma(n+\rho+1/2)\Gamma(n+\kappa+1/2)}\right]^{1/2}. \tag{3}$$

It is worth mentioning that the PT potential has an underlying SU(1,1) dynamical symmetry algebra, which admits an infinite number of energy levels. Some of them can be excited to create a CS wave packet by using an appropriate laser. These states have many classical features and tend to preserve their properties even for long evolution times. Here, we consider a displacement operator CS [25] of this potential. Construction of this CS makes use of the exponential form for the solution of hypergeometric differential equation and the correct choice of SU(1,1) generators [26]. The CS depends upon a parameter $\beta$ and can be written as [27]

$$\chi_\beta(x)=\sum_{n=0}^{\infty}d_n^\beta\psi_n(x), \tag{4}$$

where the amplitudes $d_n^\beta$ are given by

$$d_n^\beta=(-\beta)^n\left[\frac{\Gamma(\rho+n+1/2)\Gamma(\kappa+n+1/2)}{2\alpha\Gamma(\kappa+\rho+n)\Gamma(n+1)(2n+\kappa+\rho)}\right]^{1/2}. \tag{5}$$

The eigenenergy $E_n$ has both linear and quadratic terms in the quantum number $n$. The time evolution of the CS generated by the PT Hamiltonian,

$$\chi_\beta(x,t)=\sum_{n=0}^{\infty}d_n^\beta\psi_n(x)e^{-iE_nt}, \tag{6}$$

is such that, at short times, the center of the wave packet reproduces the classical motion, due to the linear term in $n$ in the energy eigenvalues. The quadratic term in $n$ is instead responsible for revival and fractional revivals [20,21], taking place on a longer time scale. In fact, it is easy to check that after the revival time $T_{rev}=\pi/\alpha^2$ (or integer multiples of it), the initial coherent state localizes back to its form after spreading. Here however, we are interested in fractional revivals, which instead take place after a time interval $(r/s)T_{rev}$, with $r$ and $s$ mutually prime integers. At fractional revival times the initial wave packet partially localizes into a superposition of spatially distributed subpackets, each of which closely resembles the initial wave packet: when $s$ is even, the wave packet breaks into $s/2$ wave packets, when instead $s$ is odd, the state is a superposition of $s$ distinct states. This means that one obtains a Schrödinger cat state, superposition of two CS with opposite phases, at one-fourth of the revival time, while four-way break up, or the so called "compasslike" state emerges at $T_{rev}/8$. As shown by Ref. [1], the latter produces sub-Planck scale structures in the phase space Wigner distribution. The behavior at fractional revival times can be derived in a straightforward way from Eq. (6) in the particular case when both $\rho$ and $\kappa$ are even. When the PT potential is symmetric ($\rho=\kappa$), the property of the Jacobi polynomial allows us to write

$$\psi_n(x)=(-1)^n\psi_n(\pi/2\alpha-x),$$

$$or\quad \psi_n(\pi/4\alpha-x)=(-1)^n\psi_n(\pi/4\alpha+x). \tag{7}$$

Using this fact at $T_{rev}/4$, a straightforward calculation yields

$$\chi_\beta(x,T_{rev}/4)=\frac{1}{\sqrt{2}}\left[e^{-i\pi/4}\chi_\beta(x,0)+e^{i\pi/4}\chi_\beta\left(\frac{\pi}{2\alpha}-x,0\right)\right], \tag{8}$$

that is, the CS is split into two parts at time $T_{rev}/4$ forming the well-known Schrödinger cat state. Each element of the superposition is proportional to the initial wave packet, even though they are situated at the opposite ends of the potential well. In the asymmetric case instead one gets

$$\chi_\beta(x,T_{rev}/4)=\chi^e_\beta(x,0)-i\chi^o_\beta(x,0);$$

$$\eta=\rho+\kappa=\text{multiple of } 4,$$

$$\chi_\beta(x,T_{rev}/4)=-i\chi^e_\beta(x,0)+\chi^o_\beta(x,0); \tag{9}$$

$$\eta=\text{multiple of } 2,$$

where $\chi^{e,o}_\beta(x,0)=\Sigma_{n,even,odd}d_n\psi_n(x)$. For the analysis at time $T_{rev}/8$, it is instead convenient to define a classical wave packet [20,21],

$$\chi^{cl}_\beta(x,t)=\sum_{n=0}^{\infty}d^\beta_n\psi_n(x)e^{-2\pi int/T_{cl}}, \tag{10}$$

which evolves with the classical periodicity $T_{cl}=\pi/(\rho+\kappa)\alpha^2$. It can be easily seen that at $t=T_{rev}/2$, the CS will revive with an extra half a period $(T_{cl}/2)$ of phase. In other words, the CS will be situated on the other side of the potential well, but with the same amplitude. The wave packet splits into two parts at time $t=T_{rev}/4$ with a relative phase of half a period $T_{cl}/2$. Four way breakup occurs instead at time $t=T_{rev}/8$, and one can see that the state at this fractional revival time becomes

$$\chi_\beta(x,T_{rev}/8)=\frac{1}{2}[e^{-i\pi/4}\chi^{cl}_\beta(x,t)+\chi^{cl}_\beta(x,t+T_{cl}/4)-e^{-i\pi/4}\chi^{cl}_\beta(x,t+T_{cl}/2)+\chi^{cl}_\beta(x,t+3T_{cl}/4)]. \tag{11}$$

One can generalize in a straightforward way to a generic fractional revival time. In fact, in this case the state can be written as

$$\chi_\beta\left(x,t=\frac{r}{s}T_{rev}\right)=\sum_{p=0}^{l-1}a_p\chi^{cl}_\beta\left(x,t-\frac{p}{l}T_{cl}\right), \tag{12}$$

where $a_p$ gives the amplitude with probability $|a_p|^2$ of each $l$ number of sub-wave packets or clones of the original wave packet. Each clone differs in phase from the original one by $T_{cl}/l$. As illustrated above, the six way breakup can be observed at the time $T_{rev}/12$.

## III. WIGNER DISTRIBUTION AND SUB-PLANCK-SCALE STRUCTURE

The Wigner quasiprobability distribution provides a clear phase-space description of a quantum state [28]. It is particularly suited for displaying quantum interference phenomena, which are associated to oscillations and to the presence of regions where the Wigner function attains negative values. From its definition, the Wigner function of the CS evolved up to time $t$ of Eq. (6) is given by

$$W(x,p,t)=\frac{1}{\pi\hbar}\int_{-\infty}^{\infty}\chi^*_\beta(x-z,t)\chi_\beta(x+z,t)e^{-2ipz/\hbar}dz. \tag{13}$$

The PT potential is an infinite array of identical impenetrable wells of width $\pi/2\alpha$ and therefore the wave function can be taken equal to zero outside the interval $[0,\pi/2\alpha]$. By imposing this fact, one finds that the following limits of integration can be taken in the above integral: in the left half of the well $(0\le x\le\pi/4\alpha)$, one has $-x\le z\le+x$, while in the right half $(\pi/4\alpha\le x\le\pi/2\alpha)$, one has $-(\pi/2\alpha-x)\le z\le(\pi/2\alpha-x)$. Let us now analyze the Wigner function of the time-evolved CS wave packet at different fractional revival times.

### A. Symmetric case

First we choose the symmetric case with parameter values $\rho=\kappa=50$ and $\alpha=2$ a.u. The CS parameter is taken as $\beta=0.6$, which corresponds to an initial wave packet with an energy distribution peaked around the level $\bar{n}=12$. The Wigner functions of the CS wave packet at different fractional revival times in phase space are shown in Fig. 2. At time $t=T_{rev}/4$ [see Fig. 2(a)] the state is a catlike state and its Wigner function can be explicitly written in the following two equivalent ways

$$W(x,p,T_{rev}/4)=\frac{1}{2}\left[W(x,p,0)+W\left(\frac{\pi}{2\alpha}-x,p,0\right)\right]-2\,\mathrm{Im}[W_{oe}(x,p)]=\frac{1}{2}\left[W(x,p,0)+W\left(\frac{\pi}{2\alpha}-x,p,0\right)\right]+\sum_{m,n}d_md_n(-1)^m\mathrm{Im}[W_{mn}(x,p)]. \tag{14}$$

The first two terms in Eq. (14) are the two localized CS

TABLE I. First row: classical action $A$, calculated from the uncertainty product; second row: size of the phase-space sub-Planck-scale structure ($a$ in a.u.) in the compasslike state ($T_{rev}/8$) for the symmetric potential ($\rho=50$, $\kappa=50$). $\beta$ varies from 0.3 to 0.8.

| | | | | | | | | | | | |
|---|---|---|---|---|---|---|---|---|---|---|---|
| Classical action, $A\sim\Delta x\Delta p$ | 0.748 | 0.867 | 1.189 | 1.904 | 3.175 | 5.58 | 9.225 | 13.123 | 18.349 | 23.256 | 30.03 |
| Area of a single tile ($a$), from Wigner plot | 1.41 | 1.2 | 0.859 | 0.57 | 0.332 | 0.194 | 0.11 | 0.078 | 0.057 | 0.045 | 0.035 |

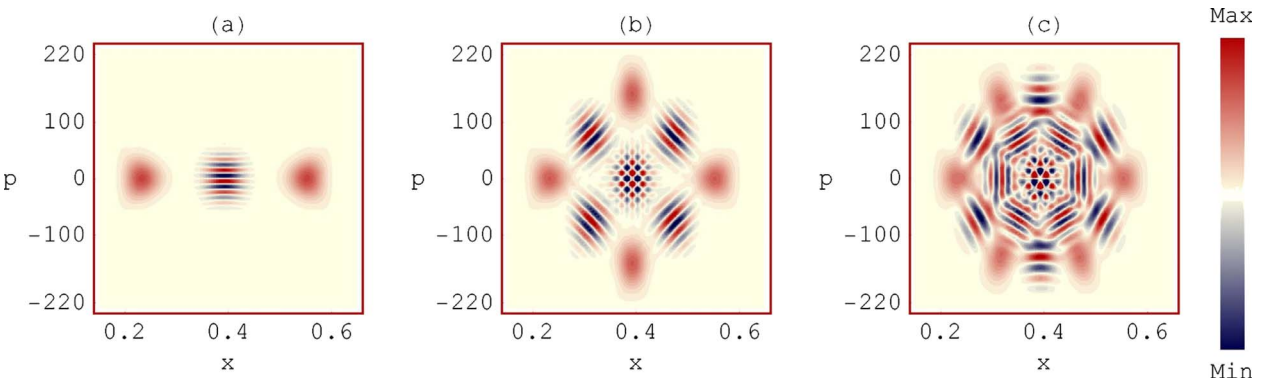


FIG. 2. (Color online) Contour plots of the Wigner distribution of the time evolution of the CS, at different fractional revival times, for a symmetric PT potential. (a) catlike state at $T_{rev}/4$; (b) compasslike state at $T_{rev}/8$; (c) benzenelike state at $T_{rev}/12$. Here we have chosen $\rho=\kappa=50$, $\alpha=2$ a.u., $\beta=0.6$, and $x$, $p$ are the conjugate variables in atomic units.

Wigner functions, situated at the left and right sides of the well. The interference fringes are associated to the third terms of the two expressions above, where the following quantities appear

$$W_{oe}(x,p) = \frac{1}{\pi\hbar}\int_{-\infty}^{\infty} \chi_{\beta}^{o}(x-z,0)\chi_{\beta}^{e}(x+z,0)e^{-2ipz/\hbar}dz,$$

$$W_{mn}(x,p) = \frac{1}{\pi\hbar}\int_{-\infty}^{\infty} \psi_{m}(x-z)\psi_{n}(x+z,0)e^{-2ipz/\hbar}dz.$$

The oscillatory interference ripples are parallel to the line joining the two split sub-CSs, i.e., the interference pattern is oscillatory only in $p$ space and also squeezed. The number of ripples decreases as the two sub-CSs come closer.

At $T_{rev}/8$ [Fig. 2(b)], the initial wave packet splits into four distinct sub-wave packets [Eq. (11)]. The Wigner function contains four distinct parts $W_1$, $W_2$, $W_3$ and $W_4$ [see Fig. 2(b)] and six interference terms, among which two diagonal partners ($W_{13}$ and $W_{24}$) overlap at the center of the phase space and generate a smaller chess-board interference pattern. This structure is the signature of sub-Planck scale structures [1,10] for a compasslike state. The central interference pattern can also be seen as the superposition of interferences of two orthogonally situated cat states, and it is formed by small tiles much smaller than the individual CS peaks.

Finally, at $t=T_{rev}/12$, the initial wave packet splits into six CSs (i.e., three pairs of catlike states), which we call a benzenelike state [Fig. 2(c)]. Sub-Planck structures also appear here in the center due to the superposition of three interference regions. A visual analysis shows that the dimension of the sub-Planck scale tiles of the compasslike state [Fig. 2(b)] is smaller than that of the benzenelike state [Fig. 2(c)]. The reason behind it is that the area of overlap increases with the number of split CSs, but we will perform a more quantitative study in the following subsection.

### B. Asymmetric case

We now discuss sub-Planck scale structures for a strongly asymmetric potential. The potential parameter values are taken as $\rho=50$, $\kappa=6$, and $\alpha=2$ a.u., as in Fig. 1 (dashed line). For the sake of comparison with the symmetric case, we choose the CS parameter ($\beta=0.88$), such that the energy distribution is again peaked around $\bar{n}=12$, as in the symmetric case. In spite of this, the interference structures are now very different. The features of the case with large asymmetry is illustrated in Fig. 3. The catlike, compasslike, and the ben-

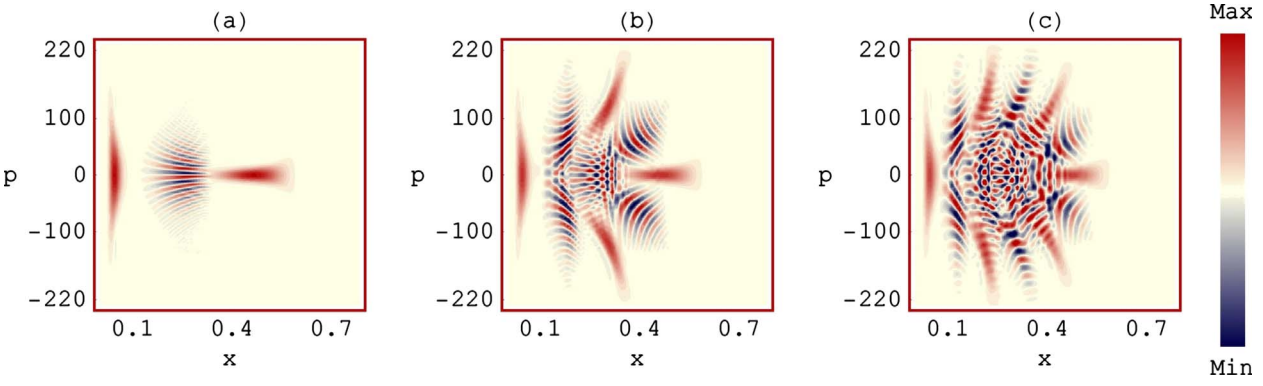


FIG. 3. (Color online) Contour plots of the Wigner distribution of the time evolution of the CS, at different fractional revival times, for a strongly asymmetric PT potential. (a) catlike state at $T_{rev}/4$; (b) compasslike state at $T_{rev}/8$; (c) benzenelike state at $T_{rev}/12$. We have chosen $\rho=50$, $\kappa=6$, $\alpha=2$ $a.u.$, $\beta=0.88$, and $x$, $p$ are the conjugate variables in atomic units.

TABLE II. Classical action $A$ and estimated dimension of the sub-Planck-scale structure for the compasslike ($T_{rev}/8$) and benzenelike state ($T_{rev}/12$), both in the symmetric (rows 1–2) and in the asymmetric potential case (rows 3–6).

| | $\rho$ | $\kappa$ | Time (scaled by $T_{rev}$) | Dimension of sub-Planck structures ($a \sim 1/A$) (a.u.) | Area of a single tile, from Wigner plot (a.u.) |
|---|---|---|---|---|---|
| 1 | 50 | 50 | 1/8 | 0.1084 | 0.110 |
| 2 | 50 | 50 | 1/12 | 0.1420 | 0.144 |
| 3 | 50 | 34 | 1/8 | 0.1278 | 0.132 |
| 4 | 50 | 34 | 1/12 | 0.2463 | 0.250 |
| 5 | 50 | 22 | 1/8 | 0.2118 | 0.225 |
| 6 | 50 | 22 | 1/12 | 0.2878 | 0.290 |

zenelike states become asymmetric and inclined toward the left boundary of the well. Since the potential well is of infinite depth, the stiffness of the potential stretches or squeezes the wave packet near the left side of the well. Moreover it spreads in $x$ space and becomes more squeezed in $p$ space. The asymmetry affects also the interference pattern of the states: the interference ripples are not anymore placed at the center, the diagonal interference patterns overlap partially and destroy the chess-board and benzenelike structures. Moreover, the interference pattern and the localized sub-CSs partially overlap and become much less distinguishable.

### C. Quantitative analysis of the sub-Planck scale structures

Let us now make a quantitative analysis and check if the smallest structures in the interference patterns, e.g., the alternate positive and negative tiles have really sub-Planck scale dimensions. Therefore we have to verify if the phase-space area occupied by the tiles "$a$" scales, as predicted, as $\sim\hbar^2/A$ ($\sim 1/A$ in atomic units), where $A$ is the classical action of the state. $A$ is approximately given by the product of the effective support of its state in position and momentum: $A \sim \Delta x \times \Delta p$, where $\Delta x = \sqrt{\langle x^2\rangle - \langle x\rangle^2}$ and $\Delta p = \sqrt{\langle p^2\rangle - \langle p\rangle^2}$.

In order to verify the scaling law, we first choose a symmetric potential ($\rho=\kappa=50$) and study the interference structures for CSs with different weighting distributions. More precisely, we vary the parameter $\beta$ from 0.8 to 0.3, which corresponds to change the position of the peak of the energy distribution from $n=32$ to $n=2$. The classical action progressively decreases for decreasing CS mean energy, while at the same time the size of the sub-Planck interference structure becomes larger. This behavior is quantitatively confirmed by Table I, where the first row gives the total phase-space area measured form the uncertainty product, while the second row shows the area of the structures measured from the Wigner plots. These data are plotted in the $\log_e$-$\log_e$ plot of Fig. 4, where they are well fitted by a straight line of slope $-1.02$. This latter plot clearly confirms the expected scaling $a \sim 1/A$ with a very good approximation, confirming also that the interference pattern has sub-Planck dimensions.

We have then extended the analysis of the size of the sub-Planck structures to situations with different symmetry, by comparing the expected dimension of the tiles from the measured phase-space area $A$ ($a \sim 1/A$), and the actual size of the tiles directly obtained from the plot of the Wigner function, for the case of the asymmetric PT potential, and for the benzene state evolved up to time $T_{rev}/12$. The results are illustrated in Table II. We have compared the compasslike and the benzenelike states for the symmetric PT potential (rows 1–2) and for two different asymmetric cases (rows 3–6). We find good agreement between the expected and the actual dimension of the sub-Planck tiles in all six cases and this fact suggests that the scaling $a \sim \hbar^2/A$ remains valid also in the asymmetric potential and for the benzenelike state, even though the range of values of $a$ considered in Table II is too small to allow us to make a firm quantitative statement [29]. We find the smallest phase-space sub-Planck structure for the compasslike state of the symmetric potential [row 1 and Fig. 2(b)]. This is a consequence of two facts that can be easily inferred from our analysis: (i) the phase-space area of the tiles is always larger in the case of the benzenelike state; (ii) the phase-space area of the tiles *increases* for increasing asymmetry of the PT potential. In the next section, following the results of [7,8] we will study the sensitivity to perturbations of the PT sub-Planck structures. One expects to have the highest sensitivity with a state possessing the finest structures in phase space and therefore the above results suggest to choose the compasslike state in the symmetric potential case for this study.

## IV. SENSITIVITY OF SUB-PLANCK SCALE STRUCTURES

An interesting feature of sub-Planck structures is that they signal the fact that the corresponding quantum state is extremely sensitive to perturbations. We now verify if this holds also for the PT sub-Planck structures found above. Here we consider two different kinds of perturbation: (i) an "internal" perturbation, corresponding to a slight change of the PT potential, which is changed from symmetric ($\rho=\kappa$) to a slightly asymmetric one ($\kappa \lesssim \rho$); (ii) an "external" perturbation, i.e., a phase-space displacement of the state, for example due to the application of a weak force. As discussed in the preceding section, we consider an initially symmetric PT potential and the compasslike state at the fractional revival time $T_{rev}/8$.

I. We set the potential parameter values $\rho=50$, $\kappa=46$, and $\alpha=2$ a.u., which give a very small asymmetry (see the solid

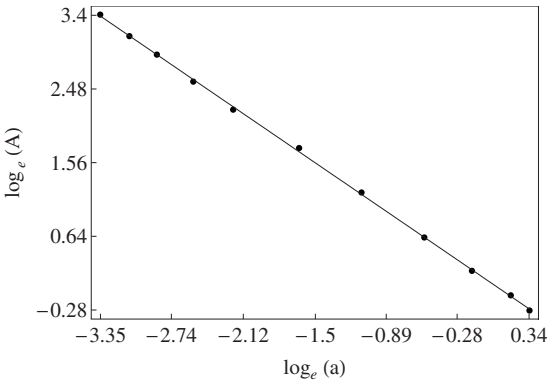


FIG. 4. $\text{Log}_e$-$\log_e$ plot of the classical action $A$ (a.u.) against the area of sub-Planck scale structures ($a$ in a.u.) in the Wigner function of the compasslike state for the symmetric PT potential with $\rho=\kappa=50$. The expected scaling law, $a\sim 1/A$, is well verified, since the data are well fitted by the line with slope −1.02.

line in Fig. 1). We compare this case with the symmetric case $\rho=\kappa=50$. We observe that the small asymmetry does not cause an appreciable modification on the phase-space behavior of the compasslike state as a whole (see the contour plots in Figs. 5(a) and 5(c) for the symmetric and slight asymmetric case, respectively). However, this is no more true if we look at the effect of the slight asymmetry on the interference pattern and we zoom in the center of the phase-space plot [see Figs. 5(b) and 5(d)]. The effect of the potential asymmetry on the interference pattern is equivalent to a phase-space shift, because one has a displacement of a single tile such that, approximately, the maximum of a tile comes to coincide with a zero of the unperturbed state. This fact just confirms that one has an extreme sensitivity with respect to

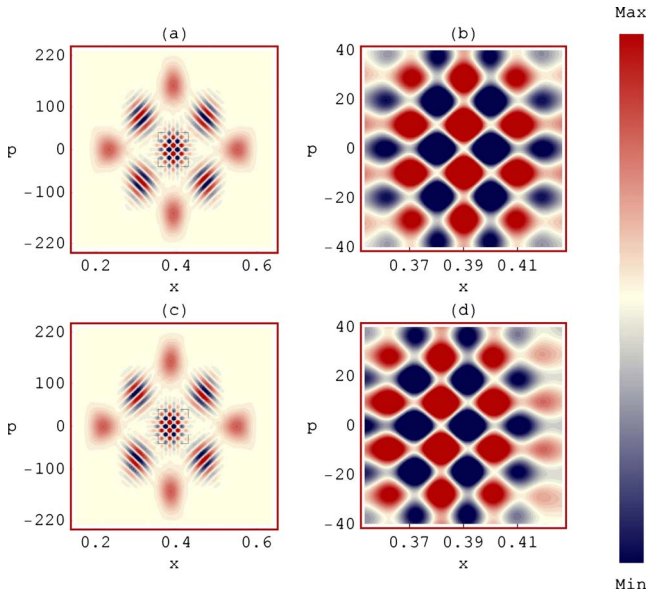


FIG. 5. (Color online) Contour plot of the Wigner function of the compasslike state for the (a) symmetric ($\rho=\kappa=50$) and (c) slightly asymmetric ($\rho=50$, $\kappa=46$), potentials. Enlarged views of the central interference regions of (a) and (c) are shown in (b) and (d), respectively. Here $\alpha=2$ a.u. and $x$, $p$ are the conjugate variables in atomic units.

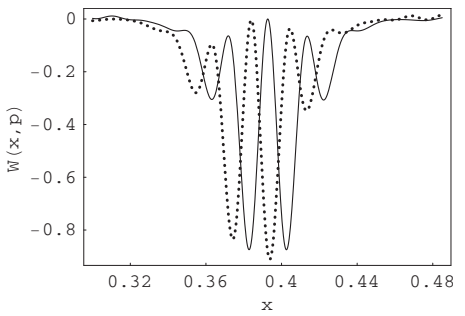


FIG. 6. Oscillations of the central sub-Planck region in $x$ space at $p=0$. Solid line refers to the symmetric case ($\rho=\kappa=50$), while the dotted line refers to the slightly asymmetric case ($\rho=50$, $\kappa=46$), as shown in Fig. 5. Here, $x$ is in atomic unit.

small changes of the potential because the two states becomes quasiorthogonal to a very good approximation ($\sim 0.1$). In fact, one has that

$$|\langle \chi_\beta^{\text{sym}} | \chi_\beta^{\text{asym}} \rangle|^2 = \int\int W_{\text{sym}}(x,p) W_{\text{asym}}(x,p) dx dp; \quad (15)$$

when the two interference patterns are displaced by a tile, one has a destructive interference effect, the above integration tends to zero and the two states become quasiorthogonal. Thus, the size of sub-Planck structures sets a sensitivity limit on probing small potential modifications.

This sensitivity is also visualized in Fig. 6, showing the section at $p=0$ of the Wigner function of the states at $T_{rev}/8$ for the two potentials. The Wigner distribution is negative, due to the nonclassicality of the state, and a shift of the

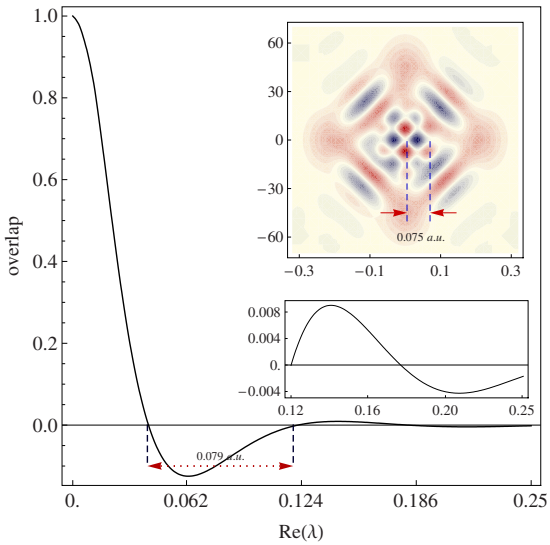


FIG. 7. (Color online) Plot of the overlap function of Eq. (17) versus the real part of the displacement parameter λ (in a.u.) at the fractional revival time $T_{rev}/8$ for $\beta=0.4$. Here $\beta'=\tanh|\lambda|e^{i\pi/4}$. The upper inset shows the central interference pattern of the Wigner function and the size of the sub-Planck structures. The lower inset shows an enlarged view of the oscillation for larger λ. The size of the sub-Planck structure is consistent with the period of oscillation of the overlap.

maximum of one curve to a minimum of the other is clearly visible. This means a sub-Planck scale shift along $x$ ($\sim 1/\Delta p$) of about 0.012 47 a.u., consistent with that in Fig. 5. A small difference in amplitudes due to the asymmetric effect is also captured in this enlarged two-dimensional (2D) view.

II. The perturbation studied above is difficult to implement in practice because one has to change to potential by keeping its PT form. In typical experimental situations a small perturbation can be applied through a weak constant force, which will physically shift the state in phase space. Therefore we consider what happens if we shift in phase space the compasslike state of a symmetric PT potential. We apply the displacement operator $\exp(\lambda K_+ - \lambda^* K_-)$ on the CS of Eq. (6), where $\lambda$ is the displacement parameter and $K_+$, $K_-$ are the SU(1,1) generators [27]. The overlap between the initial and final states in terms of the Wigner distribution is

$$|\langle \chi_\beta^{\mathrm{CS}} | \chi_{\beta'}^{\mathrm{DCS}} \rangle|^2 = \int\int W_{\mathrm{CS}}(x,p) W_{\mathrm{DCS}}(x,p) dx dp, \quad (16)$$

where $\chi_\beta^{\mathrm{CS}}$ is the initial CS evolved at time $t$ and $\chi_{\beta'}^{\mathrm{DCS}}$ is the displaced coherent state (DCS) at the same time. After a long calculation we find the DCS and the above mentioned overlap can be written as

$$\langle \chi_\beta^{\mathrm{CS}} | \chi_{\beta'}^{\mathrm{DCS}} \rangle = \sum_{n,m,p} \mathbf{D}_{m,n,p}^{\beta,\beta'} e^{-i(E_n - E_{n-m+p})t}, \quad (17)$$

where

$$\mathbf{D}_{m,n,p}^{\beta,\beta'} = \frac{\beta^{2n-m+p}(-\beta')^m(\beta')^p}{m!\,p!} \times \frac{\Gamma(2\rho+2n-m+p)\Gamma\left(\rho+n+\frac{1}{2}\right)\Gamma(2\rho-m+p+1)\Gamma\left(\rho+n-m+p+\frac{1}{2}\right)}{\Gamma(n-m+1)\Gamma\left(\rho+n-m+\frac{1}{2}\right)\Gamma(2\rho+p+1)\Gamma(2\rho+2n-2m+p)}$$
$$\times \frac{\Gamma\left(\rho+n-m+p+\frac{1}{2}\right)}{\Gamma(2\rho+n-m+p)(n-m+p+\rho)} e^{\eta(n-m+\rho/2+1/4)}. \quad (18)$$

Here $\lambda = |\lambda| e^{i\theta}$, $\beta' = \tanh|\lambda| e^{i\theta}$, and $\eta = -2\log_e(\cosh|\lambda|)$, after using the normal form of the disentanglement formula for SU(1,1) algebra [25]. We choose a symmetric potential for $\rho = 50$, $\alpha = 2$ a.u. and an initial CS parameter $\beta = 0.4$. We have plotted the overlap of Eq. (17) at time $T_{rev}/8$ (Fig. 7) versus the displacement parameter $\lambda$. One has damped oscillations which are again caused by the interference pattern of the compasslike state. The two states becomes quickly orthogonal, showing the sensitivity of the state to displacement. This oscillation is similar to the one shown by the overlap between the displaced and the undisplaced compasslike state of the harmonic oscillator (HO) case [7], with the relevant difference that here in the PT case they decay very quickly. The oscillations for larger $\lambda$ are shown in the enlarged view in the lower inset of Fig. 7. This decay of the overlap oscillations is due to the fact that for physical systems with SU(1,1) or SU(2) algebras as our PT system, a displaced coherent state does not remain a coherent state, due to the higher order terms in the Baker-Campbell-Hausdorff development of the displacement operator. Therefore, the larger the displacement $\lambda$, the more distorted the coherent state, implying that the overlap is always close to zero when the displacement is not small. The HO instead obeys the Heisenberg–Weyl algebra ($[a, a^\dagger] = 1$) and the displaced coherent state is still a coherent state, so that the overlap oscillations decay much more slowly. However the important point of our result is that, even though only one or two oscillations are visible, the period of oscillation, which gives the scale of quasiorthogonality, is extremely small. This means that the PT system is very sensitive to phase-space displacement. Moreover this sensitivity is due just to the sub-Planck structures of the compass-state. In fact, the period of the overlap oscillation is 0.079 a.u. (see the dotted arrow in Fig. 7), which is very close to the $x$-span of a sub-Planck structure of the compasslike state, equal to 0.075 a.u., as shown by zoomed view of the Wigner function in the upper inset of Fig. 7. This means that shifting a single sub-Planck tile results in the cancellation between the positive and negative contributions of the two Wigner functions, thereby making the states quasiorthogonal.

## V. CONCLUSIONS

We have shown that sub-Planck scale structures emerge in the time evolution at fractional revival times also in the PT potential. We have studied in particular the generation of compasslike states at $T_{rev}/8$ and benzenelike states at $T_{rev}/12$. We have studied both the symmetric and strongly asymmetric PT potential and we have verified that in all cases the phase-space area of the sub-Planck structures scales as $\hbar^2/A$, where $A$ is the classical action associated with the state. In particular we have seen the smallest phase-space structure (tile) is associated with that of the compasslike state of the symmetric PT potential. For this reason we have considered this state for analyzing the sensitivity of the PT system to perturbations. We have considered the effect on this state of a slight asymmetry of the potential and of a phase-

space displacement. We have seen that in both cases, the sub-Planck structures are responsible for high sensitivity because as soon as a single tile is displaced in phase space so that its maximum coincides with a minimum of the undisplaced state, one has destructive interference and the two states become approximately orthogonal.


[1] W. H. Zurek, Nature (London) **412**, 712 (2001).
[2] Ph. Jacquod, I. Adagideli, and C. W. J. Beenakker, Phys. Rev. Lett. **89**, 154103 (2002).
[3] D. A. Wisniacki, Phys. Rev. E **67**, 016205 (2003).
[4] G. S. Agarwal and P. K. Pathak, Phys. Rev. A **70**, 053813 (2004).
[5] P. K. Pathak and G. S. Agarwal, Phys. Rev. A **71**, 043823 (2005); D. Alonso, S. Brouard, J. P. Palao, and R. Sala Mayato, *ibid.* **69**, 052111 (2004).
[6] S. Ghosh, U. Roy, C. Genes, and D. Vitali, Phys. Rev. A **79**, 052104 (2009).
[7] F. Toscano, D. A. R. Dalvit, L. Davidovich, and W. H. Zurek, Phys. Rev. A **73**, 023803 (2006).
[8] D. A. R. Dalvit, R. L. de M. Filho, and F. Toscano, New J. Phys. **8**, 276 (2006).
[9] L. Praxmeyer, P. Wasylczyk, C. Radzewicz, and K. Wódkiewicz, Phys. Rev. Lett. **98**, 063901 (2007).
[10] S. Ghosh, A. Chiruvelli, J. Banerji, and P. K. Panigrahi, Phys. Rev. A **73**, 013411 (2006).
[11] J. R. Bhatt, P. K. Panigrahi, and M. Vyas, Phys. Rev. A **78**, 034101 (2008).
[12] M. Stobinska, G. J. Milburn, and K. Wódkiewicz, Phys. Rev. A **78**, 013810 (2008).
[13] J. Banerji, Contemp. Phys. **48**, 157 (2007).
[14] A. J. Scott and S. M. Caves, Ann. Phys. **323**, 2685 (2008).
[15] B. Y. Tong, Solid State Commun. **104**, 679 (1997).
[16] B. Y. Tong and N. Kiriushcheva, Phys. Lett. A **229**, 49 (1997).
[17] J. Radovanovic, V. Milanavic, Z. Ikonic, and D. Indjin, Phys. Lett. A **269**, 179 (2000).
[18] H. Yildirim and M. Tomak, Phys. Rev. B **72**, 115340 (2005).
[19] H. Yildirim and M. Tomak, J. Appl. Phys. **99**, 093103 (2006).
[20] I. Sh. Averbukh and N. F. Perelman, Phys. Lett. A **139**, 449 (1989).
[21] R. W. Robinett, Phys. Rep. **392**, 1 (2004) and references therein.
[22] G. Pöschl and E. Teller, Z. Phys. **83**, 143 (1933).
[23] S. Sree Ranjani, A. K. Kapoor, and P. K. Panigrahi, Ann. Phys. **320**, 164 (2005).
[24] J. P. Antoine, J. P. Gazeau, P. Monceau, J. R. Klauder, and K. A. Penson, J. Math. Phys. **42**, 2349 (2001).
[25] A. M. Perelomov, *Generalized Coherent States and Their Applications* (Springer, Berlin, 1986).
[26] N. Gurappa, P. K. Panigrahi, and T. Shreecharan, J. Comput. Appl. Math. **160**, 103 (2003).
[27] U. Roy, J. Banerji, and P. K. Panigrahi, J. Phys. A **38**, 9115 (2005).
[28] W. Schleich and J. A. Wheeler, Nature (London) **326**, 574 (1987); W. Schleich and J. A. Wheeler, J. Opt. Soc. Am. B **4**, 1715 (1987); W. Schleich, D. F. Walls, and J. A. Wheeler, Phys. Rev. A **38**, 1177 (1988); W. P. Schleich, *Quantum Optics in Phase Space* (Wiley-VCH, Berlin, 2001) (and references therein).
[29] The numerical study of a wider interval of values for "*a*" turns out to be problematic in the case of asymmetric PT potentials because for larger asymmetry the direct measurement of *a* from the Wigner plots became more and more unreliable.